SANDIA REPORT
SAND2012-9920
Unlimited Release
Printed November 2012

Simulation of Photovoltaic Power Output for the Salt River Project Integration Study

Clifford W. Hansen, Amanda Luketa-Hanlin, Aidan P. Tuohy, and Kristen M. Nicole

Prepared by
Sandia National Laboratories
Albuquerque, New Mexico 87185 and Livermore, California 94550

Sandia National Laboratories is a multi-program laboratory managed and operated by Sandia Corporation, a wholly owned subsidiary of Lockheed Martin Corporation, for the U.S. Department of Energy's National Nuclear Security Administration under contract DE-AC04-94AL85000.

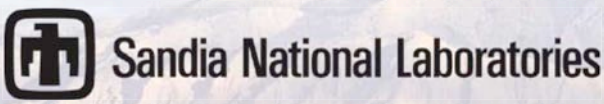

Issued by Sandia National Laboratories, operated for the United States Department of Energy by Sandia Corporation.

Available to DOE and DOE contractors from
U.S. Department of Energy
Office of Scientific and Technical Information
P.O. Box 62
Oak Ridge, TN 37831

Telephone: (865) 576-8401
Facsimile: (865) 576-5728
E-Mail: reports@adonis.osti.gov
Online ordering: http://www.osti.gov/bridge

Available to the public from
U.S. Department of Commerce
National Technical Information Service
5285 Port Royal Rd.
Springfield, VA 22161

Telephone: (800) 553-6847
Facsimile: (703) 605-6900
E-Mail: orders@ntis.fedworld.gov
Online order: http://www.ntis.gov/help/ordermethods.asp?loc=7-4-0#online

SAND2012-9920
Unlimited Release
Printed November 2012

Simulation of Photovoltaic Power Output for the Salt River Project Integration Study

Clifford W. Hansen, Amanda Luketa-Hanlin
Photovoltaic and Distributed Systems Integration Department
Sandia National Laboratories
P.O. Box 5800
Albuquerque, New Mexico 87185-1099

Aidan P. Tuohy
Electric Power Research Institute
942 Corridor Park Boulevard
Knoxville, TN 37902

Kristen M. Nicole
Electric Power Research Institute
2000 L Street NW Suite 805
Washington, DC 20036

Abstract

One year of power output was simulated at one-minute intervals for each of fourteen hypothetical utility-scale photovoltaic power plants and for the aggregate power output from a large number of distribution-connected photovoltaic systems. For utility-scale plants, the simulation first constructs one-year time series of global horizontal irradiance at one-minute intervals at each plant location, and a performance model translates irradiance and weather information to AC output power. Distribution-connected photovoltaic systems comprise a v ariety of system configurations: residential-scale rooftop systems at various tilts; commercial-scale flat-roof mounted systems; and commercial-scale ground-mounted tracked systems. For distribution-connected PV systems, the simulation estimates the time series of spatially-averaged irradiance for the region containing the systems, and the performance model is employed to estimate power aggregate power from all systems. The simulation results are validated by comparing statistics for the time series of irradiance with statistics for measured irradiance within the region.

CONTENTS

FIGURES

TABLES

NOMENCLATURE

AC	alternating current
CDF	cumulative distribution function
DC	direct current
DHI	diffuse horizontal irradiance
DNI	direct normal irradiance
DOE	Department of Energy
EPRI	Electric Power Research Institute
GHI	global horizontal irradiance
mph	miles per hour
MW	megawatt
POA	plane of array
PV	photovoltaic
RMSE	root mean square error
SF	soiling factor
SNL	Sandia National Laboratories
SRP	Salt River Project

1. INTRODUCTION

The Electric Power Research Institute (EPRI) requested Sandia National Laboratories to simulate AC power output from:

1. a set of hypothetical utility-scale photovoltaic plants of varying size with either fixed-tilt PV modules or employing single-axis tracking;
2. a collection of distribution-connected photovoltaic (DPV) power systems.

The results of these simulations are intended for use in a study by EPRI that examines the possible effects of increased levels of photovoltaic (PV) generation on bulk power variability within the Salt River Project (SRP) service territory.

For utility-scale plants, EPRI provided general guidance regarding plant location and size. Specific plant locations were chosen to coincide with available irradiance measurements from the Arizona Meteorological Network (AZMET) [1] as shown in Figure 1. Table 1 summarizes location, size and technology type for each hypothetical plant. The names of the corresponding AZMET measurement stations are retained for convenience. All plants with fixed-tilt mounting are at latitude-tilt and oriented due south; plants with tracked mounting employ single-axis horizontal roll trackers without gimbal limits, and with a tracking axis oriented due south and tilted 20° from horizontal. Modeling trackers as not having gimbal limits will tend to overestimate ramp rates early and late in the day, because the modeled power will rise more rapidly from zero (and fall more rapidly towards zero) during these time periods, than if gimbal limits were applied.

Modules representative of current technology were assumed for each type of plant. All plants employed SatCon 500kW PVS-500 inverters; the number of modules in series was determined by the DC voltage input requirements of this inverter type. All plants were configured to avoid energy loss due to inverter clipping.

Table 1. Location, Size and Mounting Technology for Simulated Plants.

Name	Latitude	Longitude	Size MW DC	Mounting	Module (no. in series)
Aguila	33.9467	111.1889	48	Fixed	FirstSolar FS272 (5)
Buckeye	33.4250	112.6833	80	Fixed	FirstSolar FS272 (5)
Coolidge	32.9778	111.6047	120	Tracked	SunPower SPR-305 (8)
Mesa	33.3867	111.8675	40	Fixed	FirstSolar FS272 (5)
Mojave	34.9672	114.6058	65	Tracked	SunPower SPR-305 (8)
Maricopa	33.0686	111.9717	60	Tracked	SunPower SPR-305 (8)
Harquahala	33.4833	113.1167	92	Tracked	SunPower SPR-305 (8)
Paloma	32.9267	112.8956	41	Fixed	FirstSolar FS272 (5)
Parker	33.8817	114.4448	100	Tracked	SunPower SPR-305 (8)
Prescott	34.5919	112.4197	44	Fixed	FirstSolar FS272 (5)
Queen Creek	33.1889	111.5300	80	Fixed	FirstSolar FS272 (5)
Roll	32.7444	113.9611	100	Fixed	FirstSolar FS272 (5)
Yuma Gila	32.7354	114.5304	120	Tracked	SunPower SPR-305 (8)
Yuma Valley	32.7125	114.7050	60	Tracked	SunPower SPR-305 (8)

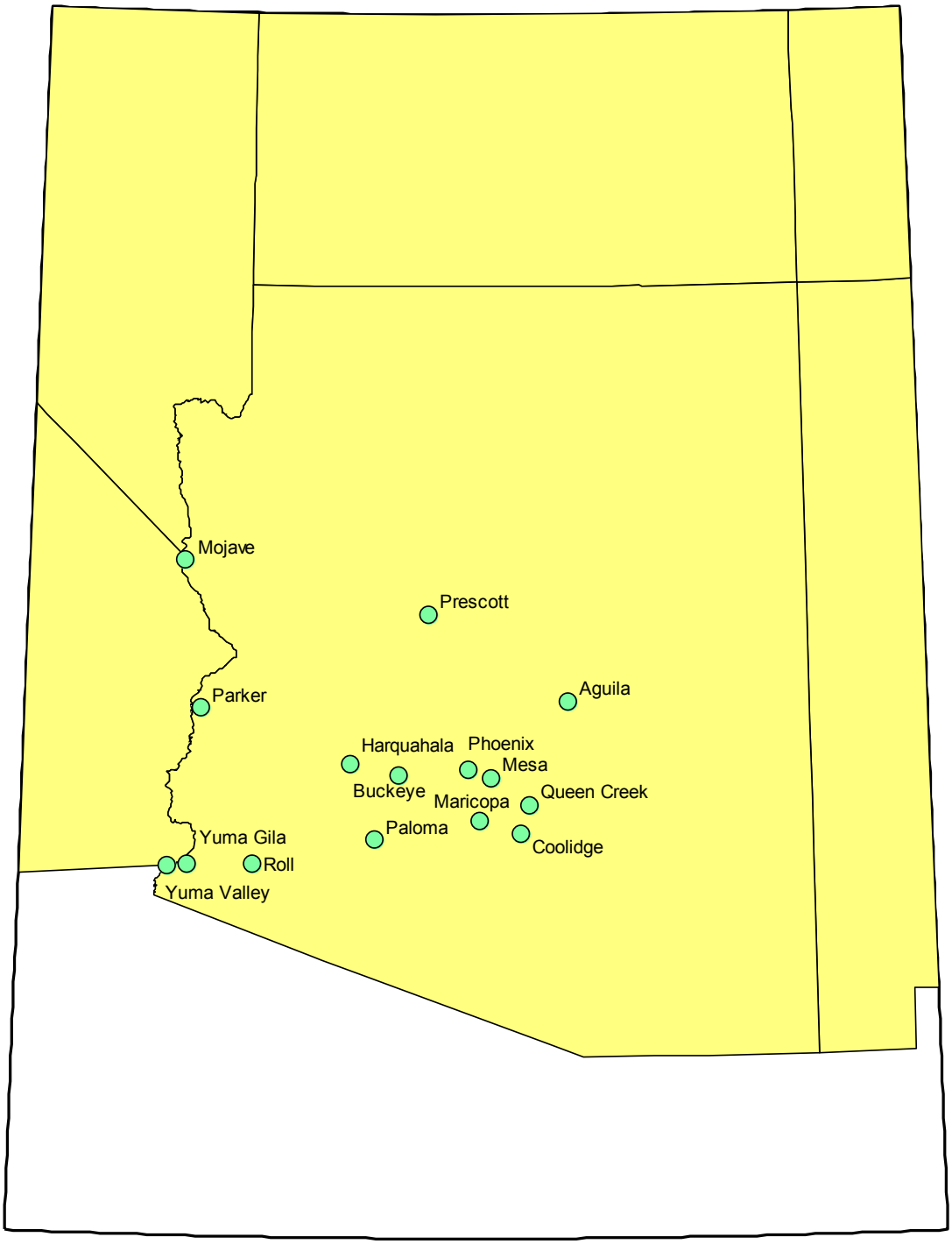

Figure 1. Map showing hypothetical PV plant locations.

For DPV, EPRI specified an aggregate capacity of 500MW over the general region of the Phoenix valley. We assumed that this aggregate capacity comprises the systems indicated in Table 2 and that all systems are designed to avoid inverter clipping. Residential systems are equally divided into five groups with tilt angles corresponding to different roof pitches: 4/12, 5/12, 6/12, 7/12 and 8/12. All systems are oriented toward the South because streets in Phoenix generally conform to a rectangular grid oriented north-south and east-west.

Table 2. Summary of Simulated Distribution-Connected PV Systems.

	Residential	**Commercial Rooftop**	**Commercial Ground Mount**
System Size	4 kW	300 kW	3 MW
Total capacity (no. of systems)	300 MW (75,000)	125 MW (417)	75 MW (25)
Module (no. in series)	FirstSolar FS-272 (5)	FirstSolar FS-272 (5)	SunPower SPR-305 (8)
Inverter	One 4kW SMA SB4000 US	Ten 30kW SatCon AE-30-60-OV-F	Six 500kW SatCon PVS-500
Mounting	Fixed tilt	Flat roof mount	Single-axis tracker Horizontal roll at 20° tilt

2. METHODOLOGY

To simulate one-minute time series of AC output from each utility-scale plant, we first simulated one-minute spatially-averaged irradiance over each plant (Section 2.1), then converted irradiance to AC power using a succession of models (Section 2.2). We used the simulated irradiance to also simulate a day-ahead irradiance forecast at hourly intervals (Section 2.3) and converted the irradiance forecast to a power forecast using the same succession of models. Finally, we simulated aggregate AC power from all DPV systems (Section 2.4).

2.1 Estimation of One-Minute Irradiance at Simulated Utility-Scale Plants

Measured, one-minute irradiance is not generally available in Arizona. Accordingly, we employed a method to simulate one-minute irradiance at the utility-scale plants that was developed and applied in an integration study [2] performed for NV Energy in 2010.

The method combines location-specific time-series of hourly average irradiance with one-minute irradiance data from other locations to simulate one-minute irradiance at the locations of the hourly data. The one-minute data should be representative of a region with climatology similar to the locations of interest, in this case the desert Southwest of the USA. The use of concurrent, hourly data at each simulation location maintains correlations in hourly average irradiance among locations, which is important for power system integration studies.

2.1.1 Available Irradiance Data

Hourly-average global horizontal irradiance (GHI) measurements are available for 2010 from the Arizona Meteorological Network (AZMET) [1], operated by the University of Arizona primarily to support agricultural research. Measurements employ LI-COR® LI200 pyranometers. We selected 14 AZMET sites near areas of interest for the EPRI study, and at which hourly data are available for 2010 (Figure 1). Hourly averages of measurements of ambient temperature and wind speed are also available at the selected sites.

EPRI made available one-minute time series of measured GHI generally around Phoenix, AZ (Figure 2). These data are measured generally between 2008 and 2011. Of the 24 sites indicated in Figure 2, two sites (H and I) had short periods of missing and/or corrupted data that were excluded from the analysis. Also, data from four additional sites (B, L, M and O) showed evidence of local shadowing; consequently, no data from these four sites were used in the analysis.

At each site, roughly 40% of the days in the one-minute data set showed clear-sky conditions for most or all of the day (Figure 3), although one site (V) showed clear sky conditions less often than most other sites, perhaps because of the mountainous terrain around this location. Reno et al. [15] recently published an algorithm that automates identification of clear-sky periods in a time series of GHI. We used this algorithm to identify days for which clear-sky conditions are present for at least 80% of daylight time to count the number of days shown in Figure 3.

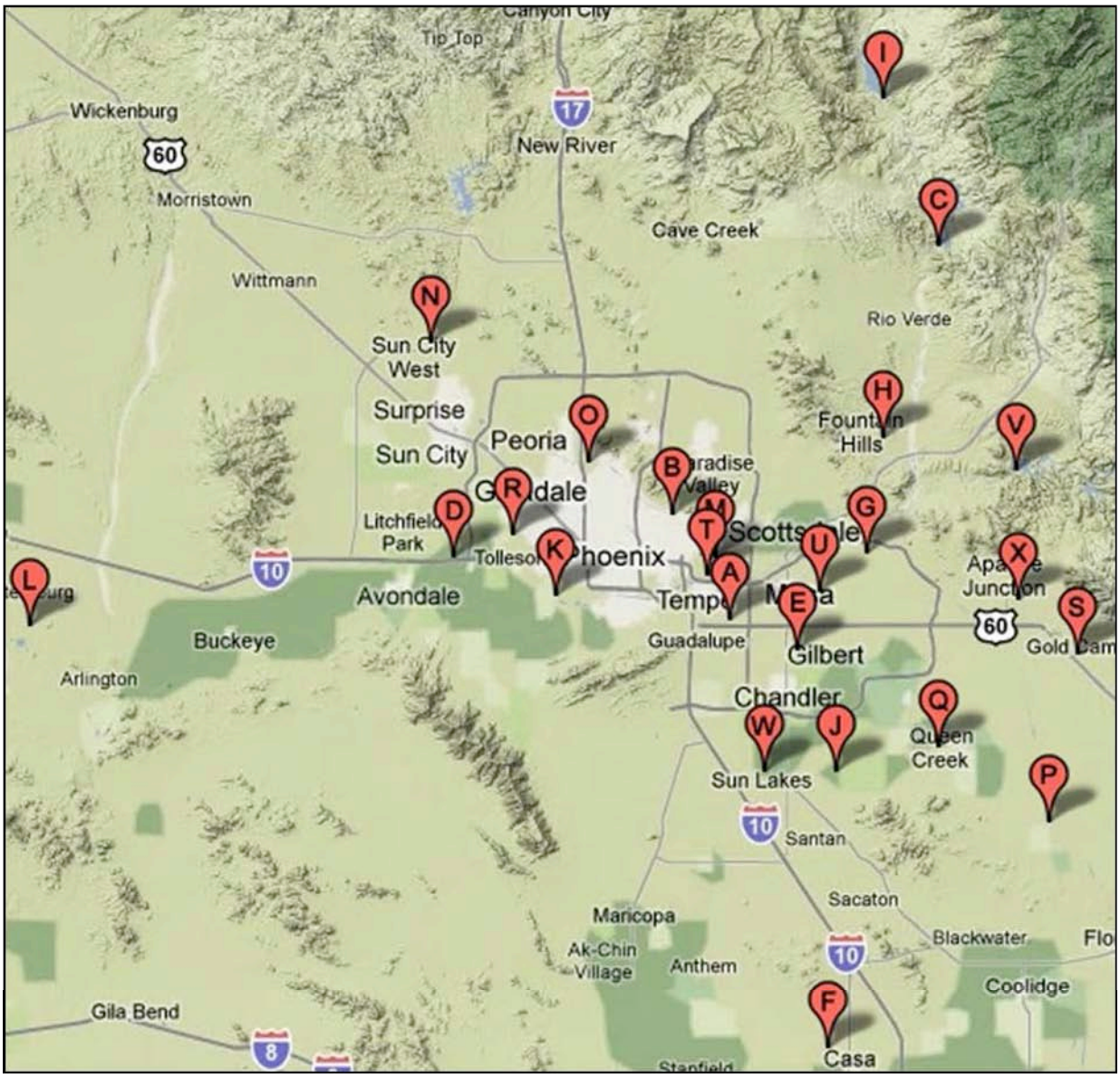

Figure 2. Locations of One-Minute Irradiance Data.

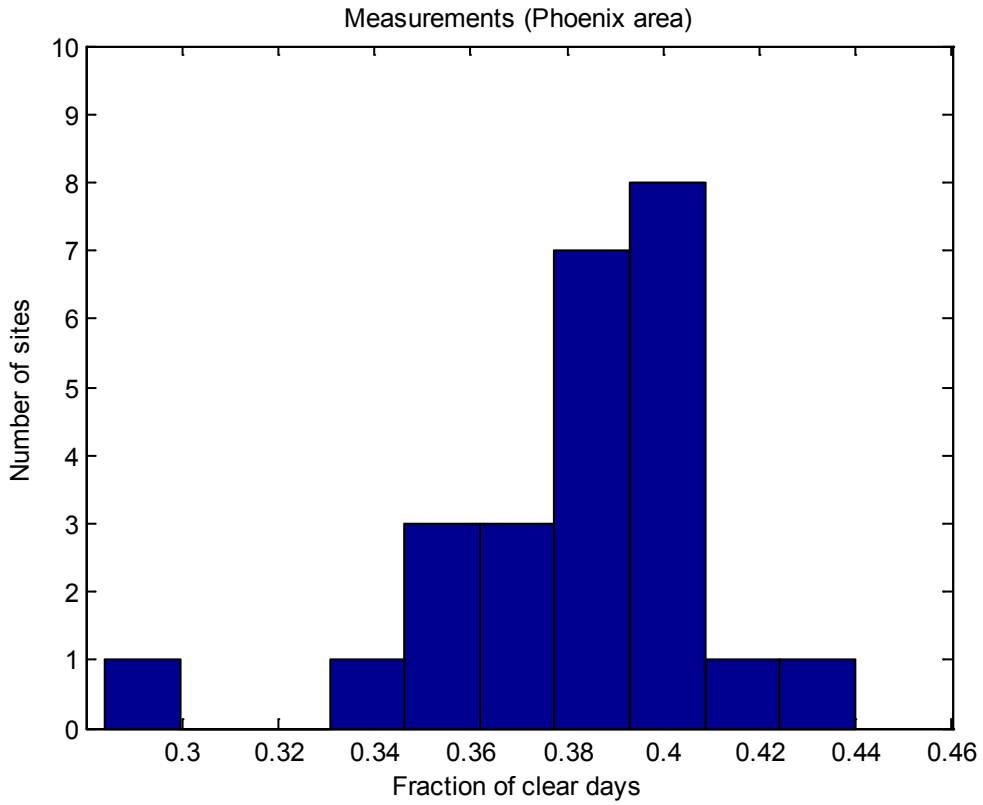

Figure 3. Fraction of Days with Clear-Sky Conditions in Measured One-Minute Data.

2.1.2 Downscaling from Hourly to One-Minute Irradiance

We downscaled from hourly to one-minute GHI one day at a time. For each calendar month, we assembled a library of one-minute irradiance "days" from the available one-minute irradiance data. To this library, we added one month of simulated clear-sky irradiance days that were calculated using the Ineichen clear-sky model [3]. Addition of a set of clear-sky days ensures that the library of irradiance days contains a clear-sky day for each day of a calendar month, which is important because of the change in the sunrise and sunset times throughout the year.

For each day of a calendar month, we selected a one-minute irradiance day from the library for each simulated plant; selection does not permit the same one-minute irradiance day to be assigned to two different plants on the same calendar day. Selection of each one-minute irradiance day was determined by minimizing the sum of the squared differences between the hourly data and the one-hour averages of the one-minute data. Selection without replacement avoids using the same one-minute irradiance day at two different plants on the same calendar day. To avoid biasing the simulated irradiance, we considered the plant locations in a random order on each calendar day. For each location, the sequence of selected irradiance days was concatenated to form a one-year time series of one-minute GHI.

2.1.3 Determining Spatial Average Irradiance

All measured irradiance data (hourly or one-minute) used in this simulation process is representative of GHI at a point (i.e., the area of the irradiance sensor, typically about 1 cm^2). In particular, the concatenated time series of one-minute GHI data for each plant's location is representative of measurement of GHI using a point sensor. Output from a PV plant correlates with the spatial aggregate irradiance over the entire plant footprint, rather than to irradiance at a point within or near the plant [4]. Consequently, spatial averages of irradiance over each plant's footprint must be determined. We estimated the spatial aggregate irradiance at each minute by using a simple moving average of the one-minute time series of GHI. We first assumed that a plant with single-axis tracking covers 10 acres per MW, that fixed-tilt plants cover 12 acres per MW, and that all plants are generally square. We determined the time, in minutes, required for a cloud to travel from one side of the plant to another assuming a constant wind speed at cloud altitude of 20 miles per hour (mph). The cloud travel time is used as the window over which the moving average of the simulated GHI is computed.

We assumed a constant cloud speed of 20 mph because we were unable to find measurements of wind speed at altitude for the region of interest. In southern Nevada measured wind at altitude generally is less than 10 m/s (22 mph) ([2], Fig. 5). Assuming that southern Nevada is a useful analog for Arizona, assuming a constant wind speed at the upper range of observations (i.e., 20 mph) will tend to overstate the largest ramps in plant output, because the cloud transits that cause these ramps are likely to require more time than is represented by the assumed cloud speed. To assess the effect of the cloud speed assumption on ramp magnitudes, we compared one-minute ramps in irradiance before and after applying the moving average to the one-minute time series. We observed that the 99^{th} percentile of one-minute ramps in plant output were somewhat reduced by the moving average, but that 95^{th} percentile of one-minute ramps was essentially unchanged. We conclude that the assumption of constant cloud speed has only a minor effect on the ramps represented in the simulation results. If significantly shorter time intervals (e.g, 1 second) were considered this conclusion would likely change.

2.1.4 Translation to Plane-of-Array Irradiance Components

Calculating DC power requires translation of spatially-aggregated GHI to the beam and diffuse components of plane-of-array (POA) irradiance. Extensive use was made of models implemented in Sandia's PV_LIB toolbox [5] for Matlab to perform this translation. We first calculated solar azimuth and elevation at one-minute intervals for each location using the *pvl_ephemeris.m* function. These values were used along with the tilt and orientation of the array to determine the angle of incidence (AOI) for both tracking and fixed systems, using the *pvl_singleaxis.m* and *pvl_getaoi.m* functions, respectively. The angle of incidence was used as a filter when calculating the beam component of irradiance; we only included values corresponding to an angle of incidence less than 90 degrees (angles greater than 90 degrees imply that the sun is behind the plane of the panel).

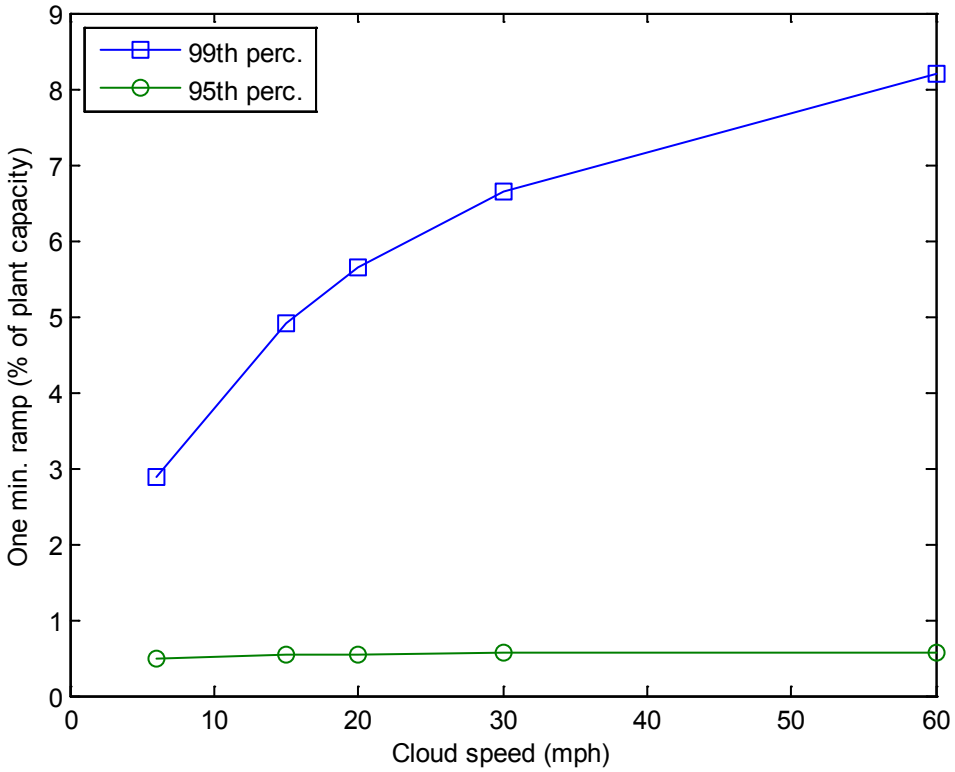

Figure 4. Percentiles of one-minute ramps in power output as a function of cloud speed.

Next, direct normal irradiance (DNI) was found using the DISC model ([6], implemented in *pvl_disc.m*), and was used to calculate diffuse horizontal irradiance (DHI) using the following equation:

$$DHI = GHI - \cos(90 - Sun\ Elevation) \times DNI$$

The diffuse POA irradiance, E_{diff}, was calculated as the sum of ground-reflected and sky components:

$$E_{diff} = E_{diff,ground} + E_{diff,sky}$$

The ground-reflected component of diffuse POA irradiance, $E_{diff,ground}$, was calculated using a simple geometric model (implemented in *pvl_grounddiffuse.m*) that assumes the ground is horizontal and uniformly reflective ([7], Eq. 22.38):

$$E_{diff,ground} = \rho GHI \frac{1 - \cos\beta}{2}$$

where β is the tilt angle and it is assumed that the ground albedo $\rho = 0.2$. The sky component of diffuse POA irradiance, $E_{diff,sky}$, was calculated using an empirical model developed by D. King of Sandia National Laboratories (implemented in *pvl_kingdiffuse.m*).

The beam component of POA irradiance, E_b, was calculated as:

$$\mathrm{E_b} = \mathrm{DNI} \times \cos(\mathrm{AOI})$$

The diffuse and beam components of POA irradiance are used in the conversion of irradiance to power.

2.2 Conversion of Irradiance to Power

Sandia's Array Performance Model (SAPM) [8] and Inverter Models [9] were used to find DC power and then AC power for each plant. SAPM simulates the DC output of PV modules. Inputs to SAPM (implemented in *pvl_sapm.m*) include a s tandard set of module parameters determined from outdoor testing, effective irradiance E_e (the irradiance converted to DC electricity by the modules), and cell temperature. Effective irradiance (suns) is calculated from the beam and diffuse components of POA irradiance ([8], Eq. 21):

$$E_e = f_1 \cdot \left[\left(E_{beam} \cdot f_2 + f_d \cdot E_{diff}\right)/E_0\right] \cdot SF$$

Here, f_1 and f_2 are empirically determined polynomials relating the solar spectral and optical influences on short-circuit current to air mass and angle of incidence, respectively, and E_0 is the conversion factor from W/m^2 to suns (i.e., $E_0 = 1000$ W/m^2. The fraction of diffuse irradiance utilized by the module is represented by f_d in the above equation. Cell temperature can then be calculated from module temperature using the following equation [8]:

$$\mathrm{T_{cell}} = \mathrm{T_{module}} + \mathrm{E_e} \cdot \Delta\mathrm{T}$$

In the above equation, ΔT is the difference in temperature between a module's back surface and a cell at an irradiance level of 1000w/m^2, typically three degrees. Module temperature, or T_{module} in the above equation, was calculated from the measured wind speed and ambient temperature data using a transient thermal model [10]; for the power calculations, one-minute temperature and wind speed values were simulated by linear interpolation between hourly averages.

The simulated DC voltage and current were used as inputs to the Sandia inverter model (*pvl_snlinverter.m*) along with a set of parameters specific to the SatCon 500kW inverter to obtain AC power produced by a single inverter. The number of inverters for each plant was determined by dividing the plant's DC capacity by the inverter capacity. The single inverter AC output was multiplied by the number of inverters to obtain AC output for the entire plant.

2.3 Emulation of Day-Ahead Hourly Forecast Power

For unit commitment and dispatch modeling, time series of forecast power production are required. We simulated day-ahead forecasts at hourly intervals for each simulated plant using the same algorithm as was developed for the integration study performed for NV Energy [2]. The algorithm stochastically generates a relative forecast error for each hour of the year, and the forecast irradiance is obtained by multiplying each hour's average simulated irradiance by the relative forecast error. Forecast errors are generated using the algorithm developed for the NV Energy integration study [2]. The forecast errors are generated differently on clear and cloudy days, consistent with the forecast methods described by Lorenz et al. [11]. For each clear day, the relative error is determined by a single normally distributed random variable with mean of one and standard deviation of 0.05. For cloudy days, forecast errors are determined for each hour using normally distributed random variables with standard deviation depending on the hour's clear-sky index value (i.e., the hourly average GHI divided by the average hourly GHI from a clear-sky model, in this analysis, the Ineichen model [3]). Lorenz et al. report relative RMSE conditional on various bins of the clear-sky index ([11], Fig. 5).

Day-ahead forecasts of hourly temperature and wind speed were simulated by a simple persistence forecast based on the recorded temperature and wind speed for each location. For January 1, 2010, the forecast temperature and wind speed were assumed equal to the measured values at each site. For successive days in the calendar, the forecast values were taken as equal to the measured values for the preceding day.

A day-ahead forecast of AC power is then obtained from the day-ahead forecasts of irradiance, temperature and wind speed by repeating the steps outlined in Sect. 2.1.4 and Sect. 2.2. Because the relative forecast error was applied to hourly-averaged simulated irradiance, no spatial smoothing was applied.

2.4 Calculation of Power from Distribution-Connected PV Systems

Power from each class of DPV system (i.e., residential, commercial rooftop and commercial ground mount) was calculated by applying the methods outlined in Sect. 2.1.4 and Sect. 2.2 to a one-minute time series of the estimated spatial average of irradiance over the Phoenix metropolitan area, along with one-minute time series of temperature and wind speed for the area. The spatial average irradiance was estimated by averaging, for each minute of the year, the measured data for the Phoenix metropolitan region (Figure 2). The use of a single spatial average is appropriate because we assume that each class of DPV system is randomly distributed around the Phoenix area. One-minute time series of temperature and wind speed were created by linearly interpolating hourly measurements from an AZMET station (Phoenix Encanto; [1]) located within the Phoenix metro area.

3. RESULTS

3.1 Illustrative Results for Utility-Scale Plants

Figure 5 illustrates the simulated one-minute GHI at one site (Aguila) and compares the simulation results with the corresponding measured hourly GHI. Reasonable agreement between simulated and measured GHI is indicated.

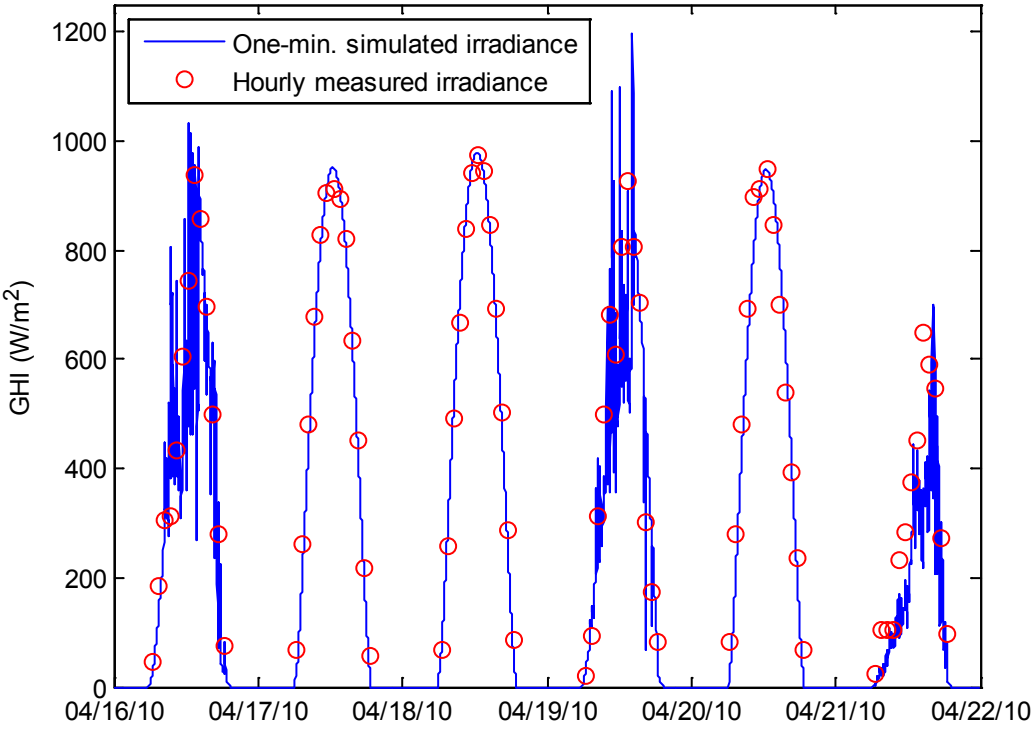

Figure 5. Illustration of simulated one-minute GHI compared with measured hourly GHI: Aguila site.

Figure 6 illustrates the simulated power for the utility-scale plant at the Aguila site by displaying five days of simulated, one-minute GHI and the corresponding AC output of the solar power plant which assumes a fixed-tilt configuration. For comparison, Figure 7 shows simulated GHI and AC output for the power plant at Mojave, where single-axis tracking is assumed. For the plant employing tracking the power vs. time curve (Figure 7) is more square in shape than the irradiance vs. time curve due to the tracking. The small variations in the power vs. time curve on clear days (e.g, 4/17/2010) result from variable wind speeds at that specific location (Mojave) on those days, which cause changes in the modeled module temperature.

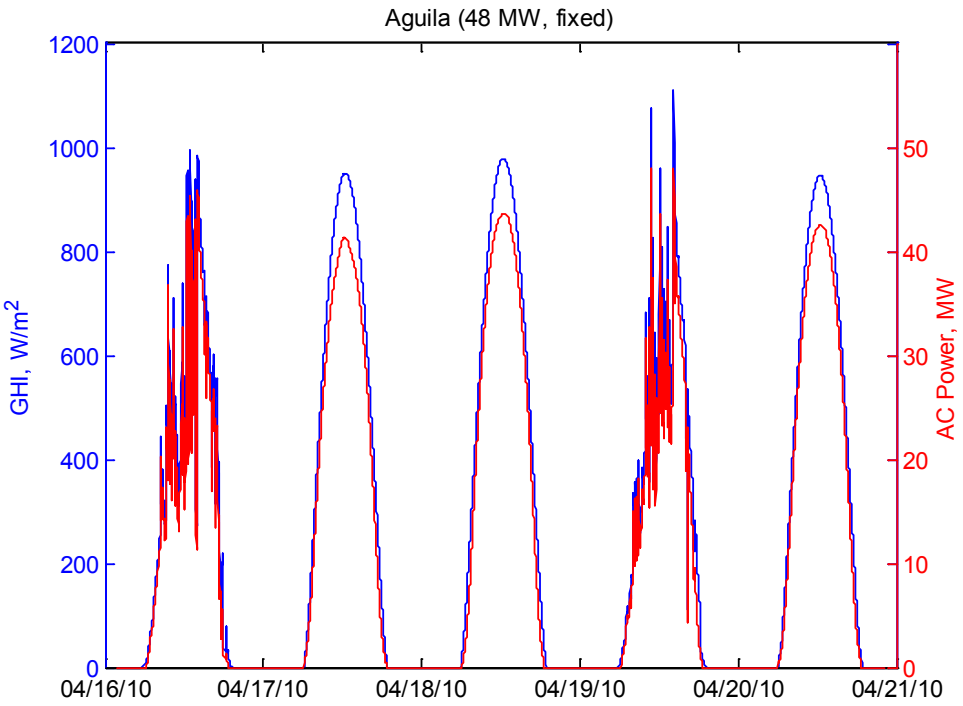

Figure 6. Five days of simulated GHI and AC output from the Aguila plant.

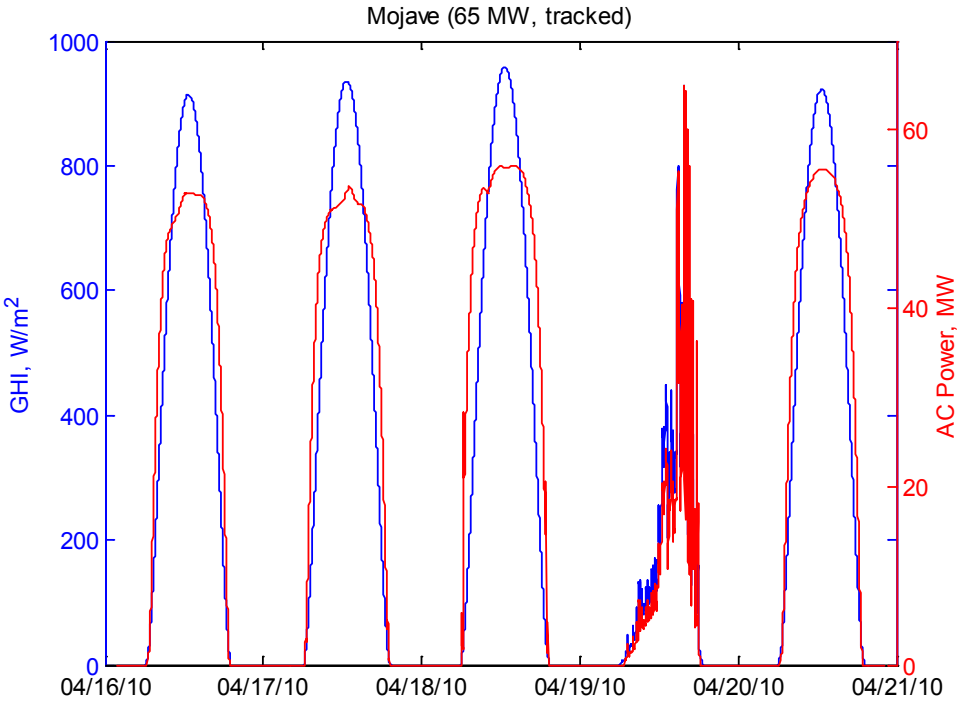

Figure 7. Five days of simulated GHI and AC output from the Mojave plant.

Figure 8 and Figure 9 show portions of the CDFs for ramps in AC power for each utility-scale site. In particular, Figure 8 displays the frequency of occurrence of large up-ramps in AC power at one-minute and hourly time scales, and Figure 9 illustrates the large down-ramps. Frequencies of occurrence are comparable for up-ramps and down-ramps of similar magnitude. For either up-ramps or down-ramps, the largest ramps approach 50% of plant capacity at both one-minute and hourly time scales; the largest hourly ramps are most likely attributable to sunrise and sunset hours, while the largest one-minute ramps are associated with cloud movement. At the 99th percentile, the one-minute ramps are roughly 15% of capacity, although the simulations display some variation among the sites. More detailed analysis of the ramping behavior of the aggregate PV output is to be reported in a forthcoming EPRI report for the SRP study.

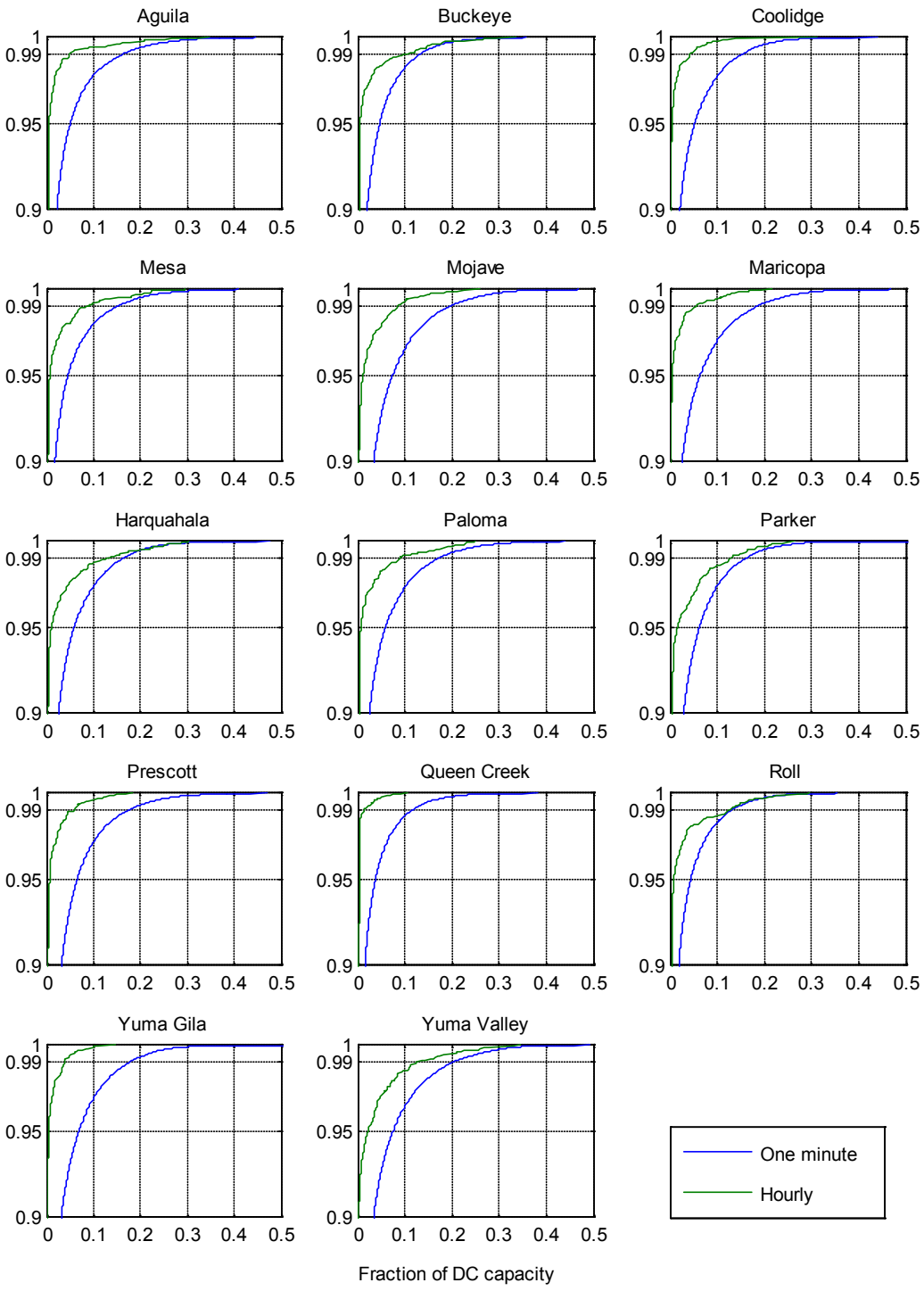

Figure 8. Distributions of one-minute and hourly up-ramps in AC power for utility-scale plants.

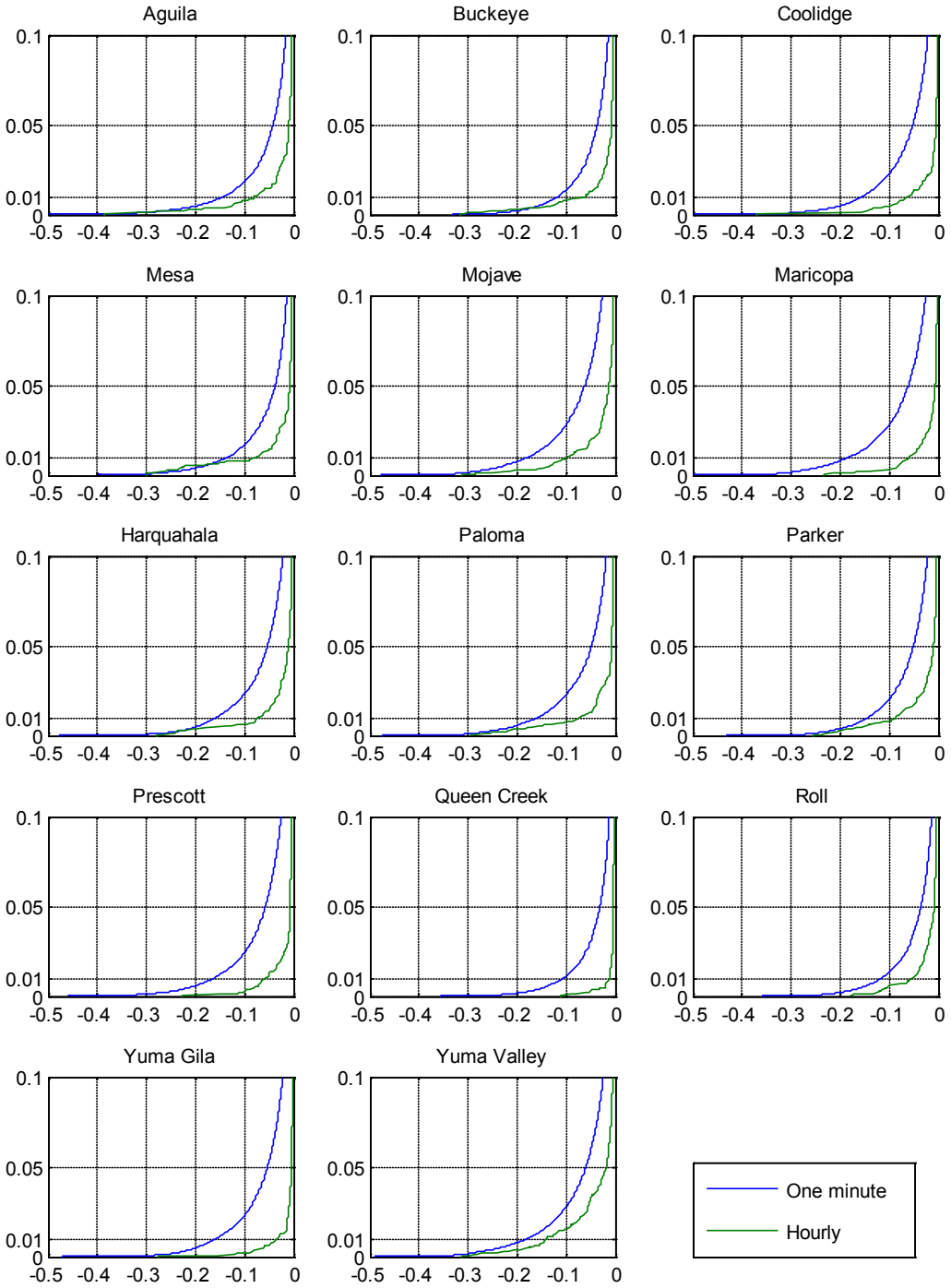

Figure 9. Distributions of one-minute and hourly down-ramps in AC power for utility-scale plants.

3.2 Illustrative Forecast Results

Figure 10 compares the day-ahead irradiance forecast with the accompanying simulated irradiance. The forecast values incorporate forecast error consistent with those reported in open literature [11]. Forecast error will be examined in more detail in a forthcoming EPRI report for the SRP study.

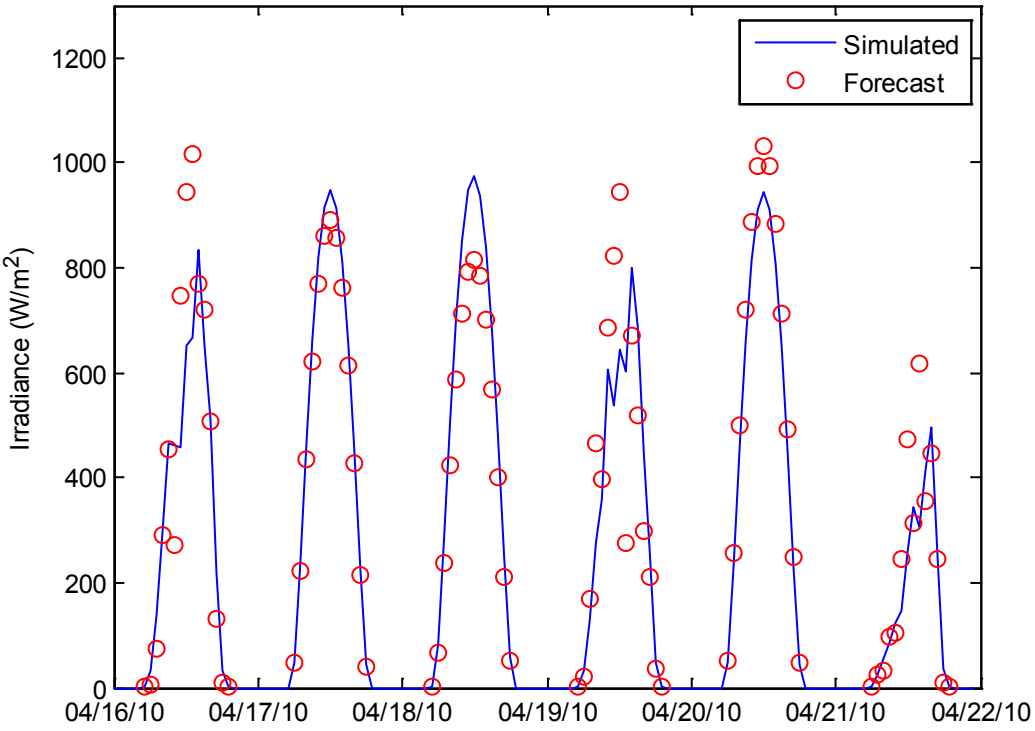

Figure 10. Illustrative Day-Ahead Irradiance Forecast.

3.3 Illustrative Distribution-Connected PV Results

Figure 11 shows aggregate simulated power from residential rooftop systems for a single day (April 16, 2010). The inset illustrates the slight variation in power that results from different roof pitches. Figure 12 shows the one-year time series of power from commercial rooftop (flat-mount) and commercial ground-mount systems. The differences in magnitude are primarily due to different assumed capacity (125MW vs. 75MW total for commercial rooftop and ground-mount systems, respectively) whereas the different profiles reflect the mounting. Commercial rooftop systems are assumed to be mounted horizontally. For these systems, power rises as the sun elevation increases, but power is lower in the summer and fall than in the spring due to higher temperatures. Ground-mounted commercial systems are assumed to use single-axis tracking and thus daily power is relatively level throughout the year.

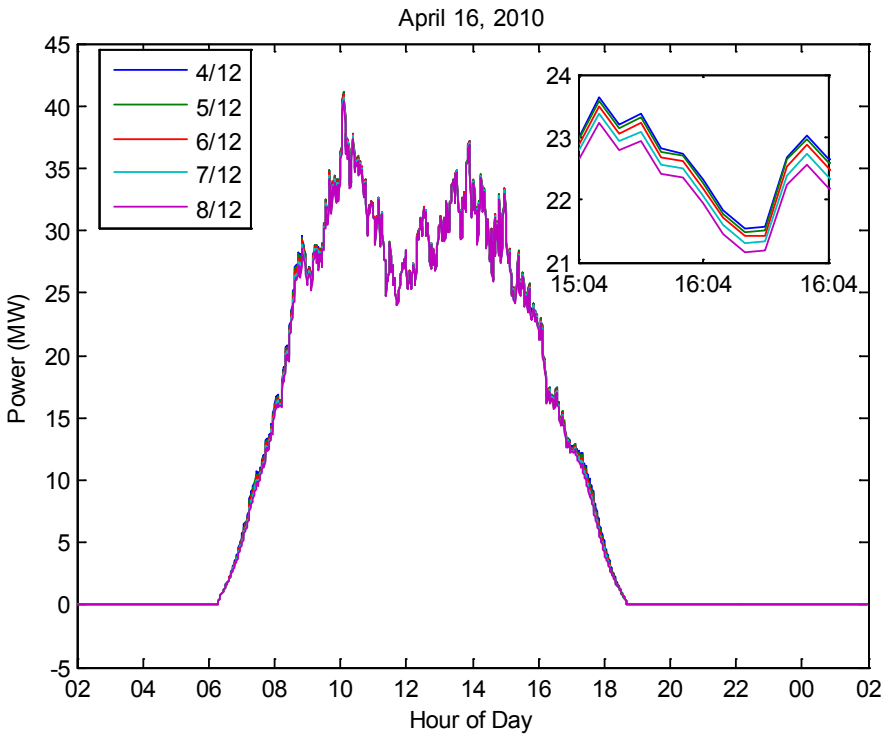

Figure 11. Aggregate Power for a Single Day from Residential PV Systems with Different Roof Pitches.

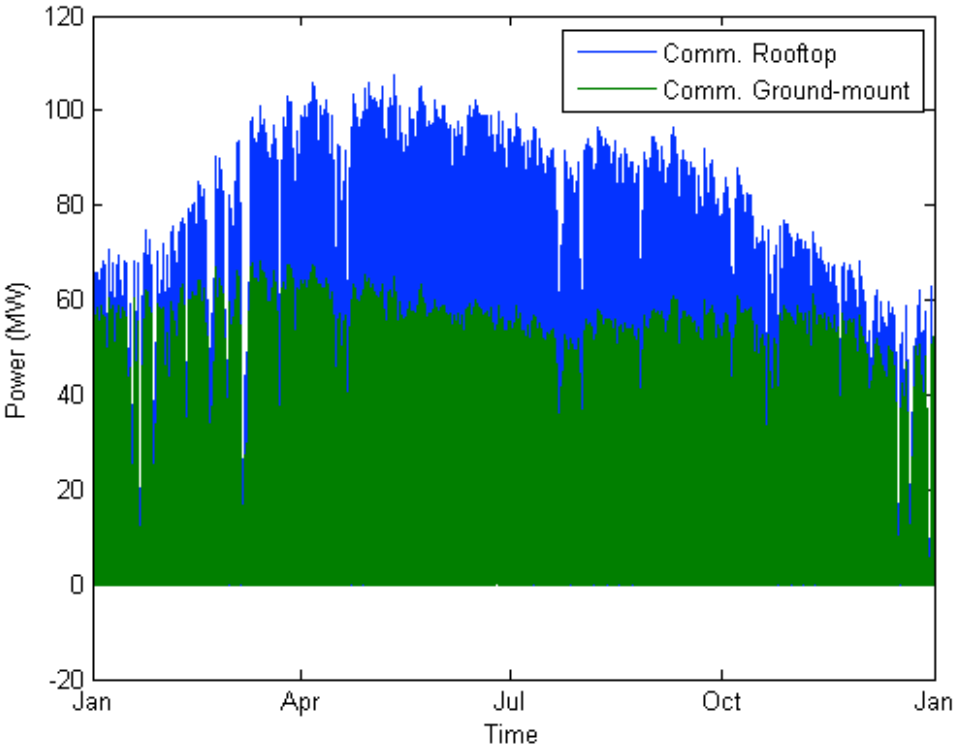

Figure 12. Aggregate Power from Commercial Rooftop and Ground-mount PV Systems.

4 VALIDATION

4.1 Validation for Utility-Scale Plant Simulations

Ideally, we would validate the simulation results by comparing the results with observations of irradiance and power during the time period of interest. However, measured one-minute irradiance is not available at the locations being simulated, and the utility-scale power systems being simulated do not exist. Consequently, validation for these results comprises comparison of statistics for irradiance between the simulated data and the hourly measured data at each location, and with the one-minute measured data for the Phoenix area. Validation thus rests on the assumption that weather at the simulation locations is similar to that observed in Phoenix.

We examine four statistics in our validation of simulated irradiance:

1. Distributions of irradiance. Agreement between simulations and measured data provides confidence that various levels of irradiance (and thus various levels of power output) occur at appropriate frequencies.
2. Distributions of changes in irradiance. Agreement between simulations and measured data provides confidence that ramps in irradiance (and thus in power) occur at appropriate frequencies.
3. Correlations between changes in clear-sky index as a function of distance between locations. Previous analyses of measured irradiance [e.g., 40] have shown that these correlations follow a general pattern, which should be evident in our simulation results. Presence of this pattern provides confidence that spatial correlations are appropriately represented.
4. Frequency of clear days. Agreement between simulations and observations provides confidence that the general characteristics of weather in Arizona are represented in our simulations.

We also examine one statistic in our validation of the accompanying irradiance forecast: the average forecast error (quantified by relative root mean square error (RMSE)) conditional on clear-sky index. We examine this statistic because comparable values are reported in the literature for current forecasting technology [11].

4.1.1 Distributions of Irradiance

Figure 13 displays cumulative distribution functions (CDFs) for GHI at each of the fourteen simulation sites. The CDFs for measured, hourly GHI for hours where GHI is nonzero are shown with the corresponding CDF for simulated one-minute GHI; no significant differences are discernible at any location. Each pair of CDFs shows agreement at almost all levels of probability, providing confidence that the simulation produces irradiance values that are consistent with measured levels. Consequently, we have confidence that output power from each

simulated plant is appropriately represented. In Figure 13 the one-minute simulation data has not been reduced to hourly averages. As a result, short-duration spikes in GHI, attributable to cloud-focusing effects [12; 13], cause the upper tail of the CDF for the simulations to extend to the right.

4.1.2 Distributions of Changes in Irradiance

Figure 14 displays CDFs for non-zero changes in hourly average GHI at each of the fourteen simulation sites. The CDFs shown in Figure 14 exclude hours where the change in GHI is zero, essentially excluding night-time periods. E ach pair of CDFs is nearly identical, providing confidence that the simulation produces irradiance time series that have changes in hourly average GHI that are consistent with the changes observed in measurements. Consequently, we may have confidence that hourly ramps in power are appropriately represented.

4.1.3 Correlations Between Changes in Clear-Sky Index

Correlation between changes in clear-sky index (i.e., GHI divided by clear-sky GHI) should decrease as the distance between locations increases [14]. Calculating these correlation coefficients quantifies what intuition suggests: two nearby locations should experience similar changes in GHI, whereas little similarity is expected for distant locations. C orrelation is calculated for changes in clear-sky index rather than for changes in GHI to remove the predictable changes due to sunrise and sunset. Correlation between changes in clear-sky index is examined, rather than for clear-sky index itself, because the objective is to judge whether concurrent increases or decreases in power output from pairs of simulated plants are appropriately represented.

Figure 15 shows correlation between changes in clear-sky index as a function of distance between locations. C lear-sky index was determined by dividing GHI by the output of the Ineichen clear-sky model at each location. The clear-sky time series was filtered to remove any times where clear-sky index exceeds 1.2, as these times generally correspond to very early morning or late evening periods where the clear-sky model is known to be inaccurate [15]. Correlation is calculated only for those portions of both time series where clear-sky index is positive.

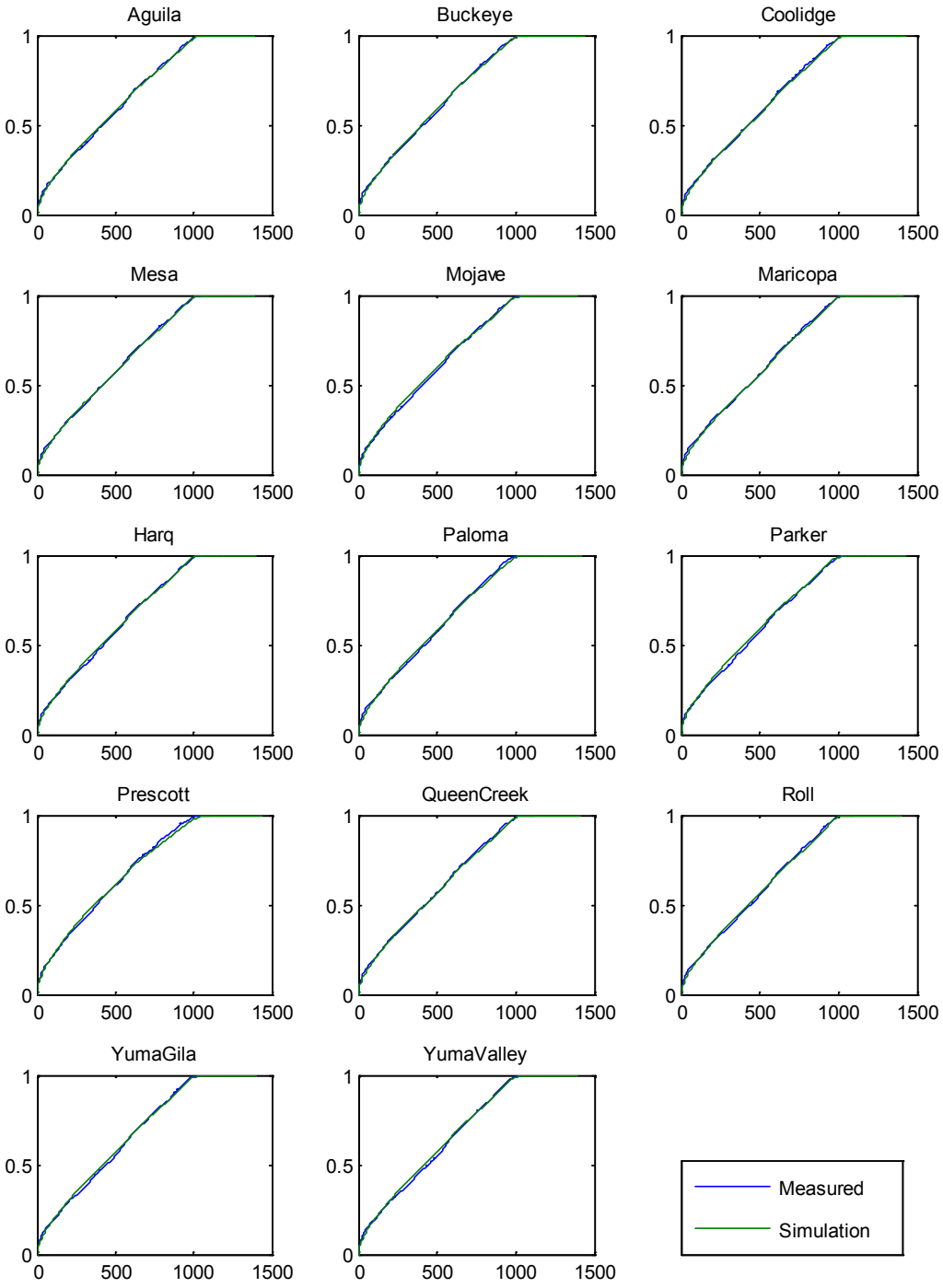

Figure 13. Cumulative distributions of simulated and measured GHI (W/m^2).

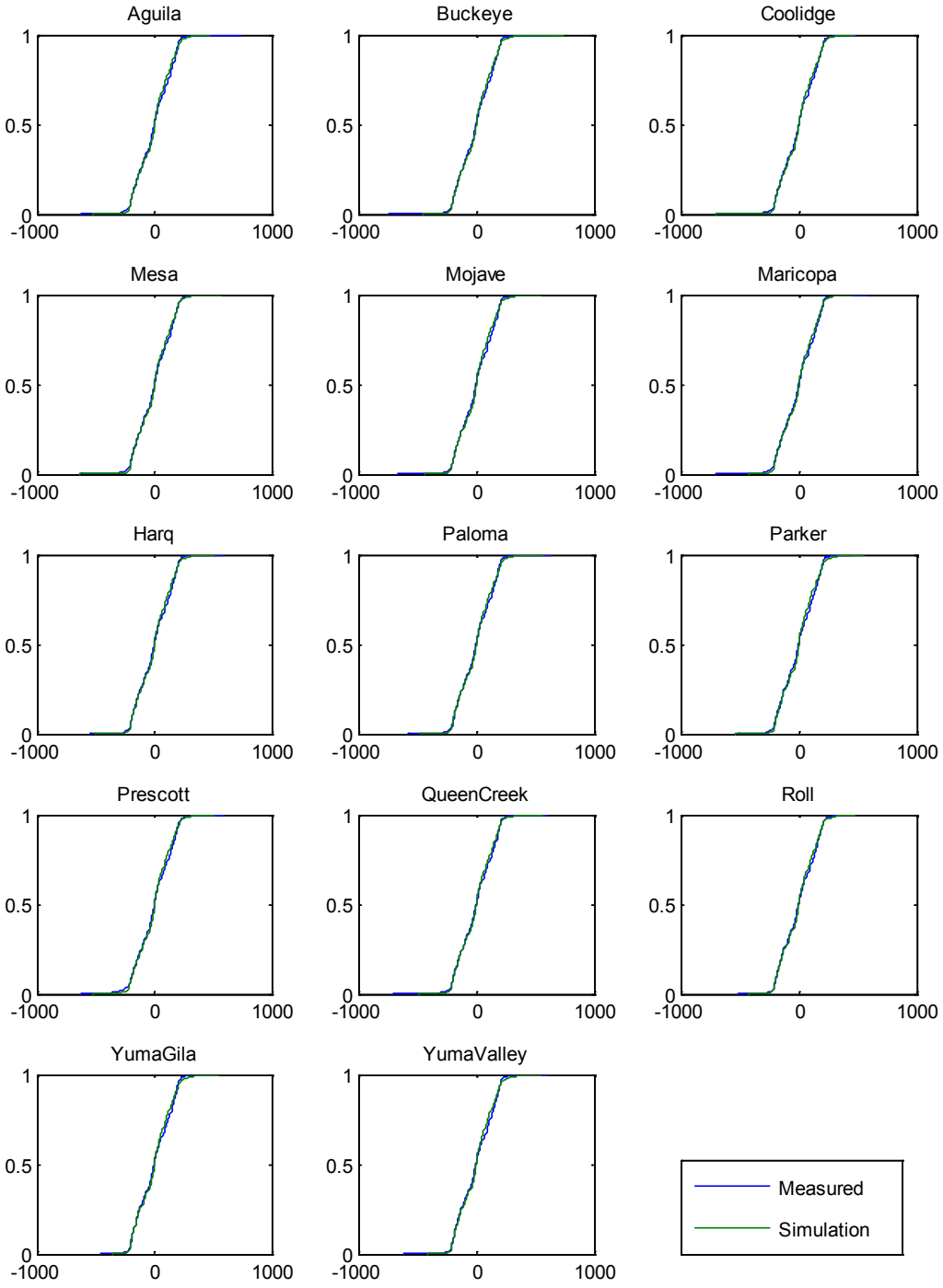

Figure 14. Cumulative distributions of simulated and observed changes in hourly average GHI (W/m^2).

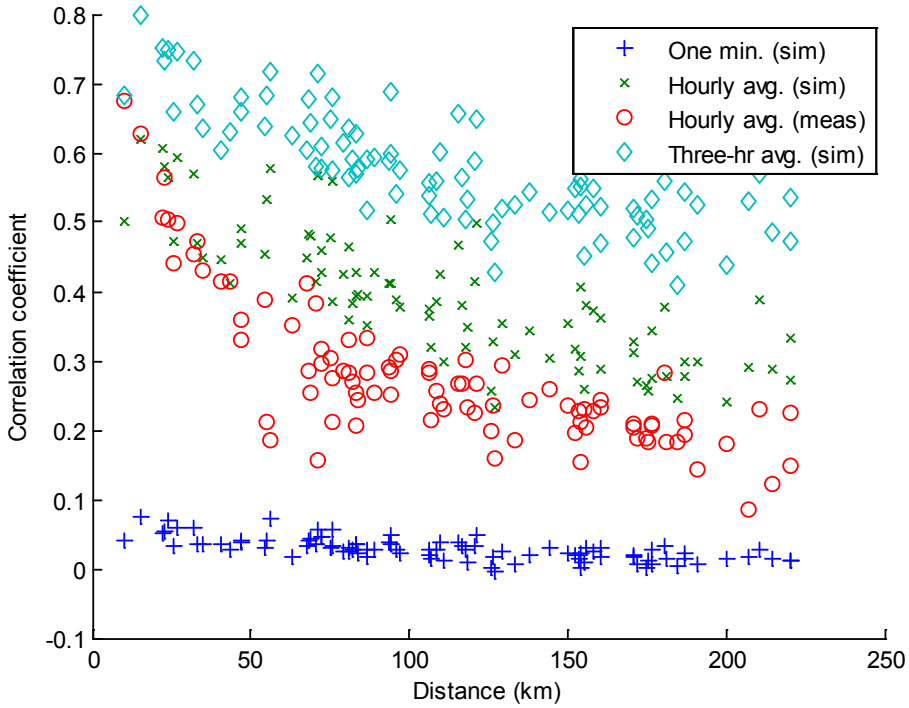

Figure 15. Correlations between changes in clear-sky index over distance.

The lack of correlation at any distance between one-minute changes in the simulated clear-sky index is consistent with results that are reported in other analyses [14]. T he decrease in correlation with increasing distance is also consistent with other analyses, as is the general increase in correlation when changes in clear-sky index are determined for longer time intervals. Because the only measured data at each location are hourly averages, we only compare correlations for changes in hourly clear-sky index between simulations and measured data.

Correlations between changes in hourly clear-sky index (i.e., hourly average GHI divided by hourly average clear-sky GHI) are generally similar for simulations and measured data, although at long distances higher correlations are seen in the simulation results than are evident in the measured data. The higher correlation at long distance is likely an artifact of using only one-minute data from the Phoenix area, which imposes a degree of similarity on distant sites that may not be present in reality. Higher correlations in clear-sky index indicate that occurrences of concurrent increases or decreases in power output from individual plants may occur more frequently in the simulations than would be expected, and thus may somewhat overstate the occurrence of larger ramps in aggregate system power.

4.1.4 Frequency of Clear Days

We also compared the occurrence of days with persistently clear-sky conditions between simulations and measured data. Reno et al. [15] recently published an algorithm that automates identification of clear-sky periods in a time series of GHI. We used this algorithm to identify

days for which clear-sky conditions are present for at least 80% of daylight time. We know of no reliable way to determine from only an hourly average GHI whether the hour is mostly clear, or not. An hour with variable conditions could have the same hourly average irradiance as an hour with generally clear conditions. Consequently, we compared the number of clear-sky days for the simulated one-minute GHI, with the number of clear-sky days evident in the one-minute measured data for Phoenix.

Figure 16 displays histograms of the fraction of days with clear-sky conditions for the simulation results and for the measured GHI in Phoenix. Similar fractions of days are observed in simulations as are evident in the measured GHI data, although the simulations show a tendency towards slightly more clear days than are evident in the measurements. At one location in Phoenix (site V), the fraction of clear day is significantly different than at other locations. The difference may be due to shadowing which may be indicated by the data, but which was not detected early in the analysis. At one simulation site (Prescott), the simulations show substantially fewer clear-sky days. We hypothesize that this results from the relatively high elevation (1583m) and surrounding mountainous terrain near Prescott, which likely corresponds to lower air temperatures and more frequent cloudy periods. These effects will be present in the measured hourly average GHI and thus will influence the selection of one-minute irradiance days for each calendar day, so that fewer clear-sky irradiance days are selected for Prescott. In contrast, all other simulation sites are at elevations below 700m and are in relatively flat desert terrain.

4.2 Validation for Simulated Forecasts

Irradiance forecasts for locations with utility-scale plants were validated by confirming that the errors generated for the simulated forecast are consistent with the errors reported for current forecasting capabilities. Actual irradiance forecasts were not available for the locations of interest. Figure 17 shows that for cloudy days (roughly 60% of the calendar year at each site) relative RMSE for our simulated forecast is statistically consistent with the errors reported in Lorenz et al. [11].

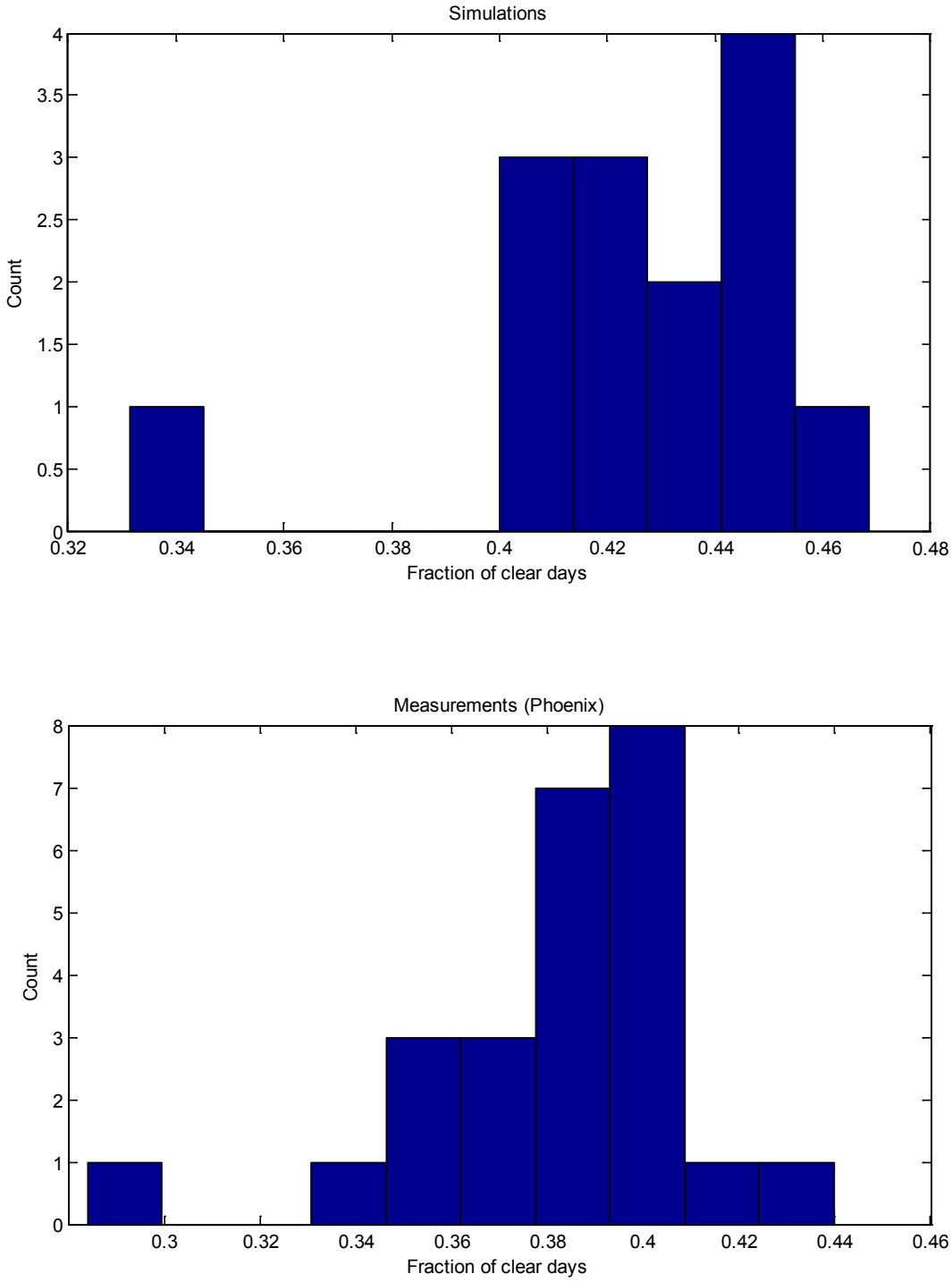

Figure 16. Histograms of the fraction of days with clear-sky conditions.

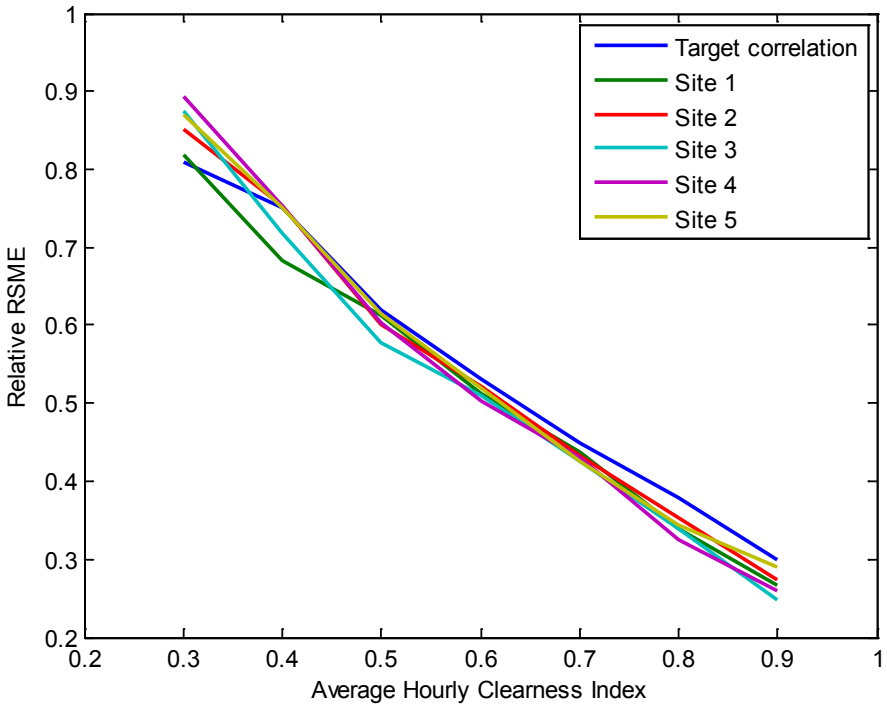

Figure 17. Forecast Error for Cloudy Days as a Function of Clear-Sky Index.

4.3 Validation for Distribution-Connected PV Simulations

We simulated power output from DPV systems by applying widely-accepted performance models [8; 9] to the spatial average irradiance measured at one-minute intervals at a large number of locations around Phoenix AZ (Figure 2). No measured output from DPV systems in the Phoenix AZ area for 2010 was available for comparison with simulation results. For a given PV module or inverter, the performance models themselves are generally accurate within a few percent over a wide range of environmental conditions. Because (i) the performance models are generally accurate, (ii) the most significant input to the calculated simulated power (i.e., irradiance) is based directly on measurements, and (iii) there is substantial empirical evidence that aggregate power from a collections of systems can be predicted from the spatial average of irradiance [4], we regard the simulation results for DPV systems as reasonable.

5. CONCLUSIONS

We simulated one-year of AC power at one-minute intervals from a set of hypothetical utility-scale photovoltaic plants of varying size, employing either fixed-tilt PV modules or single-axis tracking, and from a collection of distribution-connected photovoltaic (DPV) power systems. We also simulated an accompanying day-ahead forecast of hourly AC power for utility-scale plants such that forecast errors are consistent with errors reported for current forecasting methods.

We validated our simulation results by comparing statistics for the simulated irradiance to statistics for measured irradiance within the region of interest (Arizona, USA).

The results of these simulations are intended for use in a study by EPRI that examines the possible effects of increased levels of photovoltaic (PV) generation bulk on power variability within the Salt River Project (SRP) service territory.

4. REFERENCES

1. The University of Arizona, *AZMET: The Arizona Meteorological Network*, Retrieved from http://ag.arizona.edu/azmet/, June 2012.
2. Hansen, C.W., J. S. Stein, A. Ellis, *Simulation of One-Minute Power Output from Utility-Scale Photovoltaic Generation Systems*, SAND Report 2011-5529, Sandia National Laboratories, Albuquerque, NM, 2011.
3. Ineichen, P., and R. Perez, "A new airmass independent formulation for the Linke turbidity coefficient," *Solar Energy,* vol. 73, pp. 151-157, 2002.
4. Kuszmaul, S., A. Ellis, J. Stein, L. Johnson, *Lanai High-Density Irradiance Sensor Network for Characterizing Solar Resource Variability of MW-Scale PV System*, Proc. of the 35th IEEE Photovoltaic Specialist Conference, Honolulu, HI, 2010.
5. Sandia National Laboratories (SNL), PV_Lib toolbox for MATLAB, retrieved from http://pvpmc.org/pv-lib/, August 2012.
6. Maxwell, E. L., *A Quasi-Physical Model for Converting Hourly Global Horizontal to Direct Normal Insolation*. Golden, CO, Solar Energy Research Institute, 1987.
7. Lorenzo, E., *Energy Collected Delivered by PV Modules*, in Photovoltaic Science and Engineering 2nd ed., eds. A. Luque and S. Hegedus, Wiley 2011.
8. King, David L., W. E. Boyson, J. A. Kratochvil, *Photovoltaic Array Performance Model*, SAND2004-3535, Sandia National Laboratories, Albuquerque, NM, August 2004.
9. King, David L., S. Gonzalez, G. M. Galbraith, W. E. Boyson, *Performance Model for Grid-Connected Photovoltaic Inverters*, SAND2007-5036, Sandia National Laboratories, Albuquerque, NM, September 2007.
10. Luketa-Hanlin, Amanda, and Joshua S. Stein. *Improvement and Validation of a Transient Model to Predict Photovoltaic Module Temperature*, SAND2012-4307C, Sandia National Laboratories, Albuquerque, NM, May 2012.
11. Lorenz, E., *Irradiance Forecasting for the Power Prediction of Grid-Connected Photovoltaic Systems*, IEEE Jour. of Sel. Topics in Appl. Earth Obs. And Remote Sensing, Vol 2 pp. 2-10, Mar. 2009.
12. Nils H. Schade, Andreas Macke, H. Sandmann, and C. Stick, *Enhanced solar global irradiance during cloudy sky conditions*, Meteorologishe Zietschrift, Vol. 16, pp. 295 - 303, June 2007.
13. Yordanov, G. H., O. Midtgård, T. O. Saetre, H. K. Nielsen, L. E. Norum, *Over-Irradiance (Cloud Enhancement) Events at High Latitudes*, Proc. of the 38th IEEE Photovoltaic Specialist Conference, Austin TX, June 2012.
14. Mills, A. and R. Wiser, *Geographic Diversity for Short-Term Variability of Solar Power*, LBNL-3884E, Lawrence Berkeley National Laboratory, Berkeley, CA, Sept. 2010.
15. Reno, M. J., C. W. Hansen, J. S. Stein, *Global Horizontal Irradiance Clear Sky Models: Implementation and Analysis*, SAND2012-2389, Sandia National Laboratories, Albuquerque, NM, March 2012.

DISTRIBUTION

1 Electric Power Research Institute (electronic copy)
Attn: Mr. Aidan Tuohy
942 Corridor Park Boulevard
Knoxville, TN 37902

1 Electric Power Research Institute (electronic copy)
Attn: Ms. Kristen Nicole
2000 L Street, NW
Suite 805
Washington, DC 20036

1	MS0115	OFA/NFE Agreements	10112
1	MS0899	Technical Library	9536 (electronic copy)


Sandia National Laboratories